frontiers | Frontiers in Pharmacology

TYPE Original Research
PUBLISHED 28 April 2025
DOI 10.3389/fphar.2025.1578117



OPEN ACCESS

EDITED BY
Yurong Lai,
Gilead, United States

REVIEWED BY
Madhukiran Parvathaneni,
Harrisburg University of Science and Technology, United States
Ryuta Saito,
Mitsubishi Tanabe Pharma Corporation, Japan

*CORRESPONDENCE
Bo Liu,
513839739@qq.com

RECEIVED 17 February 2025
ACCEPTED 11 April 2025
PUBLISHED 28 April 2025

CITATION
Zhang M, Wu K, Long S, Jin X and Liu B (2025) Prediction of pharmacokinetic/pharmacodynamic properties of aldosterone synthase inhibitors at drug discovery stage using an artificial intelligence-physiologically based pharmacokinetic model.
*Front. Pharmacol.* 16:1578117.
doi: 10.3389/fphar.2025.1578117



# Prediction of pharmacokinetic/pharmacodynamic properties of aldosterone synthase inhibitors at drug discovery stage using an artificial intelligence-physiologically based pharmacokinetic model

Mengjun Zhang[1], Keheng Wu[2], Sihui Long[1], Xiong Jin[1] and Bo Liu[3]*

[1]School of Chemical Engineering and Pharmacy, Wuhan Institute of Technology, Wuhan, China, [2]Yinghan Pharmaceutical Technology (Shanghai) Co., Ltd., Shanghai, China, [3]School of Chemistry and Chemical Engineering, Shanghai University of Engineering Science, Shanghai, China

The objective of this study is to develop an artificial intelligence-physiologically based pharmacokinetic (AI-PBPK) model to predict the pharmacokinetic (PK) and pharmacodynamic (PD) properties of aldosterone synthase inhibitors (ASIs), enabling selection of the right candidate with high potency and good selectivity at the drug discovery stage. On a web-based platform, an AI-PBPK model, integrating machine learning and a classical PBPK model for the PK simulation of ASIs, was developed. Baxdrostat, with the most clinical data available, was selected as the model compound. Following calibration and validation using published data, the model was applied to estimate the PK parameters of Baxdrostat, Dexfadrostat, Lorundrostat, BI689648, and the 11β-hydroxylase inhibitor LCI699. The PD of all five compounds was predicted based on plasma free drug concentrations. The results demonstrated that the PK/PD properties of an ASI could be inferred from its structural formula within a certain error range, providing a reference for early ASI lead compounds screening and optimization. Further validation and refinement of this model will enhance its predictive accuracy and expand its application in drug discovery.

KEYWORDS

**AI-PBPK, PK/PD simulation, CYP11B2, aldosterone synthase inhibitors, machine learning**

## 1 Introduction

Primary hyperaldosteronism, a common cause of resistant hypertension and an underlying cause of cardiac and renal diseases, is usually treated with mineralocorticoid receptor (MR) antagonists (Awosika et al., 2023; Miguel et al., 2024; Verma et al., 2024). However, these drugs are not always well tolerated and can cause a counterregulatory increase in aldosterone secretion, limiting their efficacy (Bogman et al., 2017). Aldosterone is synthesized from cholesterol through a series of enzymatic steps, with the last step catalyzed by aldosterone synthase (AS) which is encoded by the CYP11B2 gene (Figure 1).

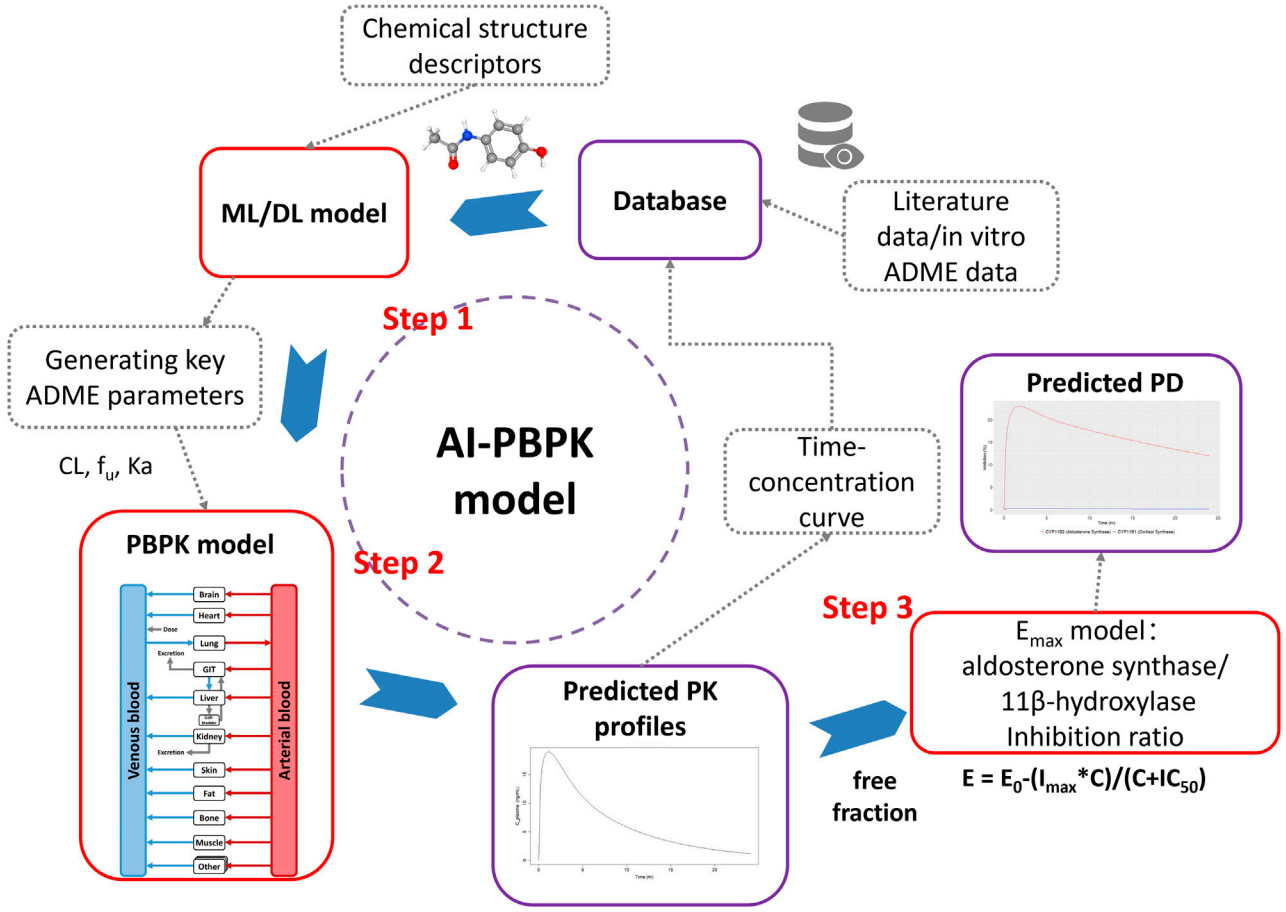


GRAPHICAL ABSTRACT
Steps for predicting a compound's PK using the AI-PBPK model and predicting enzyme inhibition by combining it with the $E_{max}$ model are shown. In Step 1, the compound's structural formula is input into the AI model to generate key ADME parameters and physicochemical properties of the compound. In Step 2, these parameters are used in the PBPK model to predict PK profiles of the compound. In Step 3, a PD model is developed to predict the inhibition rate of aldosterone synthase and 11β-hydroxylase based on the plasma free concentration of the drug.

Researchers have targeted AS inhibition to curb the production of aldosterone (Andersen et al., 2012; Hargovan and Ferro, 2014). Yet, most aldosterone synthase inhibitors (ASIs) also exert an effect on 11β-hydroxylase. This enzyme, encoded by the CYP11B1 gene, facilitates the synthesis of cortisol, a steroid hormone structurally related to aldosterone (Nishimoto et al., 2023). This lack of selectivity of ASIs leads to side effects. Thus, compounds which selectively inhibit AS without affecting 11β-hydroxylase are needed. To identify an ideal ASI, a *de novo* design approach could be applied. But it can be extremely time-consuming and costly. A more feasible approach, i.e., comparison and optimization of the pharmacokinetic (PK) and pharmacodynamic (PD) properties and selectivity of existing ASIs (Mazzieri et al., 2024) might provide a solution. A drug's PK/PD properties can be experimentally determined, as done conventionally. But again, this process usually is long and resource-intensive (Haid and Reichel, 2024). To shorten the drug discovery process, we developed an artificial intelligence (AI)-augmented physiologically based pharmacokinetic (PBPK) model to predict the PK and PD of ASIs.

A classical physiologically based pharmacokinetic model is well established, and it integrates physiological characteristics with a drug's physicochemical properties to predict the drug's behavior across different populations (Peters, 2021; Balhara et al., 2022). It helps optimize selection of the drug's dosage and dosage form, as well as assessment of efficacy of the drug, by simulating its absorption, distribution, metabolism, and excretion (ADME) (Zou et al., 2020). Key input parameters for the classical PBPK model include human physiological parameters and molecule-specific parameters. To ensure accuracy of the classical PBPK model, comprehensive collection of the above parameters on software platforms such as GastroPlus and Simcyp are required (Arafat et al., 2021; Ezuruike et al., 2022). But at the drug discovery stage, molecule-specific parameters are often constrained by extensive *in vitro* experiments (Li et al., 2024). In recent years, the use of AI-based approaches to predict physiological parameters has emerged as a promising alternative. A number of web-based ADMET prediction tools have been developed, including ADMET-AI (Swanson et al., 2023), SwissADME (Daina et al., 2017), pkCSM (Azzam, 2023), XenoSite Web (Dang et al., 2020), and ADMETlab 3.0 (Fu et al., 2024). These tools offer advantages such as high efficiency, simplicity, and easy data interpretation by chemists. However, they have limitations such as single predictive function, incapability to predict PK and PD of compounds, and failure to

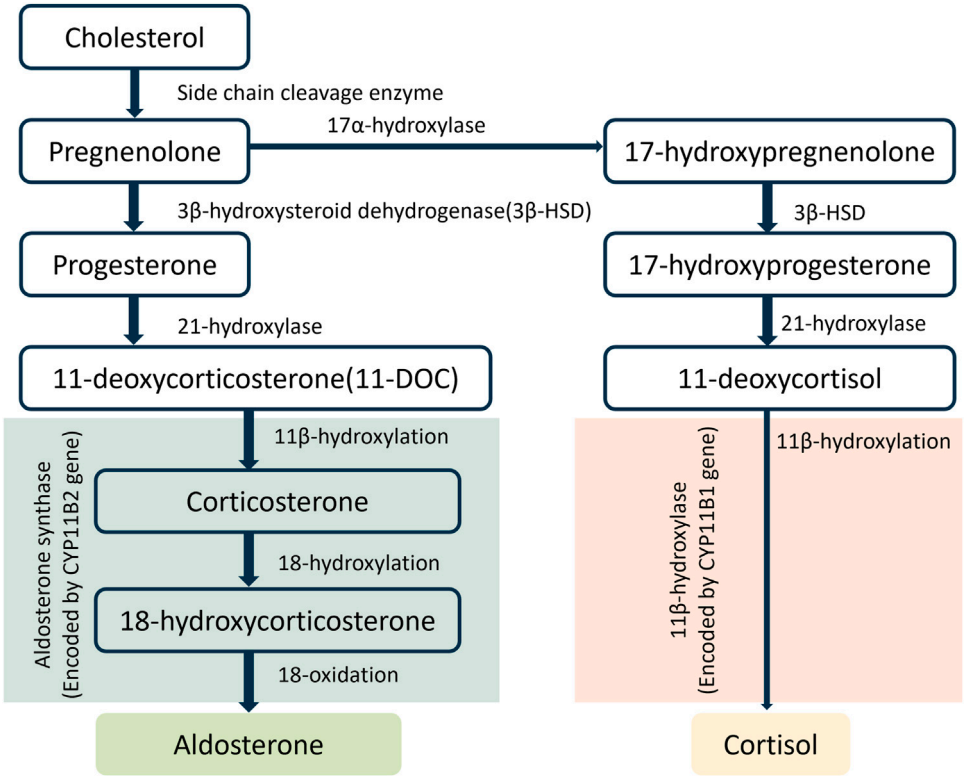


FIGURE 1
Biosynthetic pathways of aldosterone and cortisol.

derive physiologically relevant information from the structural formula of compounds.

To address these limitations, on our web-based B$^2$O Simulator® (B$^2$O stands for Bioavailability, Bioequivalence, Optimization) platform, we developed a general AI-PBPK model, which integrates the PBPK model with machine learning (ML) and deep learning (DL), enabling a comprehensive prediction of a drug's PK/PD profile from its molecular structure. At the drug discovery phase, when there are not enough drug-specific parameters to support the classical PBPK model, machine learning can be used to predict them based on the drug's structural formula. With the aid of ML, the classical PBPK model can screen more potential candidate compounds at the preclinical drug discovery phase, avoiding unnecessary testing of a large number of candidates and shortening the process of advancing the candidates to preclinical studies. The AI-PBPK model facilitates the simulation and prediction of the behavior of diverse drug candidates *in vivo*. With it, we can better understand how drugs interact with the physiological systems, and predict their distribution, metabolism, and elimination in the body more efficiently (Chen et al., 2021; Chou and Lin, 2023), and reduce the dependence on experimental data at the screening phase. Therefore, the AI-PBPK model can have a broad perspective in facilitating drug safety assessment, efficacy prediction, formulation optimization, and therapy personalization (Marques et al., 2024; Visan and Negut, 2024).

In this study, an AI-PBPK model was built and used to predict the PK/PD properties of five ASIs, assisting the identification of the optimal candidate. In general, the predicted results are in good agreement with experimental observations, with occasional discordance, indicating the applicability of our model. With further improvement of the robustness of our AI-PBPK model, it is expected to be widely used in drug discovery.

# 2 Methods

## 2.1 Overall workflow of model building

The workflow for predicting the PK profiles of a compound using the AI-PBPK model is shown in Figure 2. It consists of four steps: model construction, calibration, validation, and simulation. To identify a selective ASI with high potency, we selected Baxdrostat, an ASI currently with the most published research data, as the model drug. After constructing the ASI model, we predicted the PK parameters of Baxdrostat and compared the predictions with publicly available clinical trial data (Bogman et al., 2017; Freeman et al., 2023). The model was then calibrated by adjusting key parameters based on the comparison. Subsequently, we conducted external validation of the model using publicly available clinical PK data of two other ASIs, i.e., Dexfadrostat and Lorundrostat, with the next most publicly available clinical PK data. By comparing the predicted results with clinical data, we assessed the predictive performance of the AI-PBPK model for ASIs (Mulatero et al., 2023; Shimizu et al., 2024). Finally, the model was used to predict the PK profiles of all five compounds, i.e., Baxdrostat, BI689648, Dexfadrostat, Lorundrostat, and LCI699 (osilodrostat phosphate), an inhibitor of the

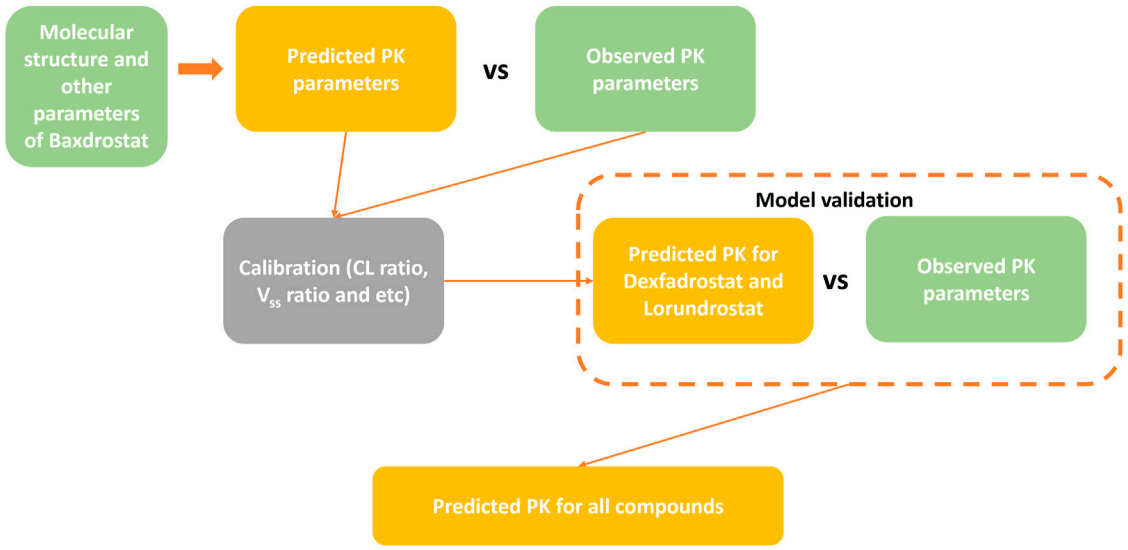


FIGURE 2
Workflow for predicting PK profiles of compounds using the AI-PBPK platform.

11β-hydroxylase. LCI699 was first approved as an orphan drug for the treatment of Cushing's disease by the European Medicines Agency in 2020, and it also received FDA approval in the same year. In this study, it was used as a control (Papillon et al., 2015; Dormoy et al., 2023; Valentín-Goyco et al., 2023).

The model used to predict PD of the five compounds is an adaptation of Macdougall's nonlinear model (Macdougall, 2006; Bogman et al., 2017), which is widely employed in dosage-response analyses. First, it is necessary to calculate the free plasma drug concentration based on the previously predicted plasma drug concentrations of all compounds, and then construct a PD model based on the free plasma drug concentration. The pharmacodynamic endpoint is mainly a compound's inhibition of AS versus inhibition of 11β-hydroxylase. The ratio of a drug's $IC_{50}$ (half-maximal inhibitory concentration) toward 11β-hydroxylase to that toward AS is defined as its selectivity index (SI).

## 2.2 Literature search

Using PubMed, Google Scholar and ClinicalTrials.gov with keywords such as aldosterone synthase inhibitor, CYP11B2, and compound name (e.g., CIN-107 and MLS-101), we compiled the aforementioned five compounds, listed in Table 1. Their associated PK/PD data were either found in the collected literature or extracted from the official website of the investigating company (Shimizu et al., 2024). The SMILES codes and structural formulae for all five compounds were obtained from PubChem (https://pubchem.ncbi.nlm.nih.gov/).

## 2.3 Machine learning and PBPK/PD modeling

### 2.3.1 Machine learning

Machine learning was used on the $B^2O$ Simulator® platform to predict drug-specific parameters. Gilmer's Message Passing Neural Networks (MPNNs) model (Gilmer et al., 2017), a subclass of graphical neural networks (GNNs) (Wu et al., 2021), is particularly useful for analyzing the chemical structure of a compound and predicting its pharmacological properties (Tang et al., 2023), such as fraction unbound in plasma ($f_{up}$), blood to plasma ratio (bpr), steady-state volume of distribution ($V_{ss}$), and gastrointestinal absorption constant (gi-ka) (Jiménez-Luna et al., 2021). The apparent clearance was also predicted using the M5P algorithm (Wang and Witten, 1997; Freitas et al., 2015). A detailed discussion of the performance of the underlying ML model and the use of the model to generate key compound parameters can be found in a previous article using the platform (Wu et al., 2024).

### 2.3.2 Data sources for machine learning

Five ADME parameters, namely, $f_{up}$ ($f_{up}$ = 1-ppbr; ppbr, plasma protein binding ratio), $CL_{app}$ ($CL_{app}$ = $V_{ss}$*0.693/half-life), $V_{ss}$ ($V_{ss}$_per kg), gi_ka (gi_ka = 2*$P_{eff}$/radius of the small intestine; Log ($P_{eff}$) = 0.6795Log ($P_{app}$)-0.3355), and bpr, were modeled by an ML approach. The diameter of the small intestine is 2.5 cm (Helander and Fändriks, 2014), thus its radius is 1.25 cm. Data for ppbr, $V_{ss}$, half-life and $P_{app}$ were obtained from the Therapeutics Data Commons (TDC) database. The Python package 'PYTDC' was installed and the corresponding dataset was used in this package. The bpr data were obtained from Mamada's work (Mamada et al., 2021). The five datasets consist of two vectors of molecular structure shown by the SMILES code and the corresponding ADME parameters for each molecule. Most of the data sources for ML come from the TDC database (datasets: ppbr, TDC. PPBR_AZ, size: 1797; $V_{ss}$, TDC. $VD_{ss}$_Lombardo, size: 1,130; half-life, TDC. Half_Life_Obach, size: 667; $P_{app}$, TDC. Caco2_Wang, size: 906; bpr, Mamada's work, size: 461) (Huang et al., 2021; Mamada et al., 2021).

### 2.3.3 PBPK/PD modeling

In the study, the whole-body PBPK model (Wendling et al., 2015; Wendling et al., 2016) was used, which consists of 14 tissue

TABLE 1 Essential data related to all five aldosterone synthase inhibitors.

| Compound | SMILES code | Alias | Company | Highest R&D status | Target | Available data |
|---|---|---|---|---|---|---|
| Baxdrostat | CCC(=O)NC1CCCC2 = C1C = NC = C2C3 = CC4 = C(C=C3)N(C(=O)CC4)C | CIN-107, RO-6836191 | CinCor, AstraZeneca PLC | Phase 3 | Aldosterone synthase | PK; PD (Bogman et al., 2017; Freeman et al., 2023) |
| Dexfadrostat | C1CC(N2C = NC = C2C1)C3 = CC = C(C=C3)C#N | DP-13, (R)-Fadrozole (Damian Pharma), DP13 | Damian | Phase 2 | Aldosterone synthase | PK; PD (Rigel et al., 2010; Weldon et al., 2016; Mulatero et al., 2023) |
| Lorundrostat | CC1 = CC = C(C=C1)C2 = CN = NC(=N2)N3CCN(CC3)CC(=O)NC4CCC(CC4)NC(=O)C | MLS-101, MT 4129 | Mineralys, Mitsubishi | Phase 3 | Aldosterone synthase | PK; PD (Laffin et al., 2023; Mineralys Therapeutics, 2023; Shimizu et al., 2024) |
| BI-689648 | COCC1 = CC(=CN = C1)C2 = CC3 = C(N=C2)N(CCC3)C (=O)N | — | Boehringer Ingelheim | — | Aldosterone synthase | PD (Weldon et al., 2016) |
| LCI-699 | C1CC2 = CN = CN2C1C3 = C(C=C(C=C3)C#N)F | Osilodrostat, Osilodrostat phosphate (JAN/USAN), 5YL4IQ1078 (UNII code), LCI-699-NX, Isturisa, イスツリサ | Novartis, Recordati SpA et al. | Approved for listing | 11β-hydroxylase | PD (Weldon et al., 2016) |

Drug data updated as of September 2024.

compartments, including lungs, heart, brain, muscle, fat, skin, spleen, pancreas, liver, stomach, intestine, bone, kidney and other parts of the body, and two blood compartments (arterial and mixed venous). Assuming equilibrium of drug distribution in tissues and plasma, the degree of distribution was characterized by the blood partition coefficient ($K_p$). The rate equation for the tissue compartment is as follows (Equation 1):

$$\frac{dA_T}{dt} = \frac{Q_T}{V_{VEN/ART}} \cdot A_{VEN/ART} - \frac{Q_T}{V_T K_p} \cdot A_T \quad (1)$$

Where $A_T$ denotes the drug amount (mg), $V_T$ is the volume (L), and $Q_T$ is the blood flow (L/h) for the 14 different tissues. $A_{VEN/ART}$ and $V_{VEN/ART}$ are the amount (mg) and volume (L), respectively, of either mixed venous blood (for the lungs) or arterial blood (for tissues other than the lungs).

Additionally, the PD model describes the correlation between the plasma free drug concentration (plasma drug concentration $*f_{up}$) and the inhibition of AS and 11β-hydroxylase. The *in vitro* inhibition assay evaluated the inhibitory effect of an ASI on the activities of the two enzymes by measuring the enzymatic conversion of 11-deoxycortisol to cortisol for CYP11B1, and 11-deoxycorticosterone (11-DOC) to aldosterone for CYP11B2, and was presented as the inhibition constants of both enzymes by the free base of the ASI (Shimizu et al., 2024). Thus, based on the free plasma drug concentration of the ASI and the corresponding inhibition constants of the compound on both enzymes, i.e., the $IC_{50}$ in this study (Table 6), PD modeling was performed separately for each enzyme. The Exposure-Response (ER) relationship is as follows (Equation 2):

$$E = E_0 - \frac{I_{max} * C}{C + IC_{50}} \quad (2)$$

Where $C$ is the plasma concentration, $E_0$ is the percentage change from baseline in plasma aldosterone concentration at $C = 0$ (theoretically 0%), and $I_{max}$ is the maximal inhibitory effect, which is typically 100% and indicates complete inhibition.

### 2.3.4 Design of simulation studies

Once the required parameters of Baxdrostat were predicted with the ML model, the constructed PBPK model was used to simulate the drug's PK profiles. The model was then calibrated appropriately based on the differences between the simulated results and the observed data. Following calibration, Lorundrostat and Dexfadrostat were selected to validate the model, and the fitting effect was evaluated by comparing the simulated outcomes with observed values. Upon validation, the single ascending dose (SAD) and multiple ascending dose (MAD) PK simulation of all drugs at dosages of 0.5 mg, 1 mg, 3 mg, 10 mg and 30 mg was selected, and the corresponding PD was simulated based on the obtained PK parameters. The dosing interval for all multiple doses was 24 h. Due to the high dosage of Lorundrostat in the clinical trials, the existing dosages of 5 mg, 10 mg, 20 mg, 50 mg and 100 mg in the clinical trials were used for SAD simulation, and dosages of 3 mg, 12.5 mg, 50 mg, and 100 mg were selected for MAD simulation. The PK and PD properties of the compounds at different dosages were analyzed and compared to determine the optimal combination of PK, PD, and dosage for the candidate drugs.

## 2.4 Software

The PBPK model was built, fitted and used for prediction using the web-based B²O Simulator® at https://simulation.b2osim.cn/signin. To access the AI-PBPK module, users must register and log in, and then input the chemical structure to predict a drug's PK parameters. The maximum serum concentration reached by a drug in the body and the area under the curve are calculated within a confidence interval (2.5%–97.5%). When the predicted data are less than 1/2 or more than twice of the observations from clinical studies,

the deviation is considered significant. All data and graphs were generated using Microsoft® Excel 2021 (64-bit) and R version 4. 3.0 software.

# 3 Results

## 3.1 Simulation, calibration, and validation of PK

### 3.1.1 Simulation of Baxdrostat's PK

The SMILES code for Baxdrostat (CCC(=O)NC1CCCC2 = C1C = NC = C2C3 = CC4 = C(C=C3)N(C(=O)CC4)C), together with the codes of the other four drugs (Table 1), were entered into the AI-PBPK platform to generate ADME and physicochemical parameters shown in Table 2. Baxdrostat's $f_{up}$ was from Bogman's work (Bogman et al., 2017). The simulated PK parameters of a single dose of 2.5 mg (same as the clinical trial dosage) of Baxdrostat and the observed data (Freeman et al., 2023) are shown in Table 3. The simulated drug exposure values, which represent the relationship between plasma drug concentration and time, are lower than the observed mean exposure values. Drug exposure is primarily reflected through indicators such as the area under the concentration (AUC)-time curve, maximum plasma concentration ($C_{max}$), and time to reach maximum concentration ($T_{max}$). The simulated PK profiles and observations for a 2.5 mg single dose of Baxdrostat are shown in Figure 3. The observed and predicted Mean Absolute Error (MAE), Mean Squared Error (MSE), Root Mean Square Error (RMSE) and R-Square ($R^2$) values are 7.81, 73.0, 8.54 and 0.54, respectively. Since the simulated results deviated significantly from the observed data, the model was calibrated.

### 3.1.2 Calibration of Baxdrostat's PK

The Kp_scaler is a scaling factor applied to modify the Kp values, which represent the tissue/blood partition coefficient. The Kp_scaler calibrates the predicted Kp values to better fit experimental data or improve the model's accuracy. The size of Kp_scaler varies based on the predicted $V_{ss}$_per Kg. The simulated $AUC_{0\text{-}24}$ (157.25 ng*hr/mL) of Baxdrostat was smaller than the observed value (365.79 ng*hr/mL), suggesting that the model overestimated the distribution of the drug in the tissue, resulting in lower simulated blood drug concentrations than the observations. Therefore, by adjusting the Kp_scaler to an extent, the drug distributed into the tissues was reduced, thereby bringing the simulated drug concentration in the blood to be closer to the observed value. The simulated plasma elimination half-life (≈6 h) was shorter than the actual one (28.37 h). The drug's predicted clearance ($CL_{app}$ = 14.83 L/h) was higher than the observed value (2.5 mg Baxdrostat, $CL_{app}$ = 3.28 L/h), suggesting that the actual drug clearance is faster than predicted. By reducing the predicted $CL_{app}$, the biological half-life was prolonged, bringing the modeled values closer to the observed ones. The final calibration for parameters was Kp_scaler * 0.85 and $CL_{app}$/4.7. The PK curve for Baxdrostat after calibration is shown in Figure 3, and it can be seen that the calibrated curve is closer to the observed one. The observed and predicted (after calibration) MAE, MSE, RMSE and $R^2$ values are 2.13, 10.87, 3.30 and 0.83, respectively. These two calibration coefficients were also applied to the other compounds. The drugs' parameters after calibration are shown in Table 4. The PK parameters generated after Baxdrostat calibration can also be seen in Table 3. The $AUC_{0\text{-}24}$ and $C_{max}$ are closer to the observed values after calibration.

### 3.1.3 Model validation with Lorundrostat and Dexfadrostat

After calibration, the predictive ability of the model was further validated by testing Lorundrostat and Dexfadrostat on it. Figure 4 shows the predicted and observed PK results for Lorundrostat and Dexfadrostat as semi-logarithmic curves. The hollow markers in the figure are observations and the solid lines are predictions. The predicted plasma concentrations of the drugs Lorundrostat and Dexfadrostat for validation were consistent with the concentration profiles observed in the literature at the initial stage after the first dose. But the plasma concentrations at the elimination stage of Lorundrostat were high and the rates of elimination slowed for both single and multiple doses, while the plasma concentrations of Dexfadrostat at the elimination stage was low for single and multiple doses and the elimination rates was fast. However, most of the ratios of predicted-to-observed $AUC_{0\text{-}24}$, $C_{max}$, and $T_{max}$ for single-dose and multiple-dose administration were within 1/2 to 2-fold (Table 5), except the $C_{max}$ of Dexfadrostat at 4 mg for SAD, and 4 mg, 8 mg, and 16 mg for MAD were not within the 2-fold error range. The coefficient of determination ($R^2$) of the predicted and observed values of $AUC_{0\text{-}24}$ and $C_{max}$ was 0.986 and 0.960, respectively (Figure 5). The simulation was based on a single virtual healthy subject. The results of the analyses showed that the model reasonably predicted drug exposure within a certain error range and is of great value for candidate screening.

## 3.2 Simulation of PK for all five compounds

After model validation, dosages of 0.5 mg, 1 mg, 3 mg, 10 mg, and 30 mg were selected for SAD and MAD PK simulation for Baxdrostat, BI689648, Dexfadrostat, and LCI699. Due to the large dosage of Lorundrostat in the clinical trials, single dose of 5 mg, 10 mg, 20 mg, 50 mg and 100 mg, and multiple doses of 3 mg, 12.5 mg, 50 mg and 100 mg were selected for PK simulation. The PK simulation results of all the compounds are shown in Figure 6. The plasma drug concentration profiles of all the compounds increased in a dosage-dependent manner as shown by the plasma drug concentration graphs for single and multiple doses. The predicted $AUC_{0\text{-}24}$ and $C_{max}$ values for all the compounds are provided in Supplementary Table S1, which shows that under both single and multiple doses conditions, the $AUC_{0\text{-}24}$ for Baxdrostat, BI689648, and Dexfadrostat is higher than that of LCI699 at equivalent doses; while the $C_{max}$ of LCI699 is slightly higher than that of Dexfadrostat at the same dosage, its rapid elimination resulted in a comparatively lower $AUC_{0\text{-}24}$ than that of Baxdrostat, BI689648, and Dexfadrostat at the same dosage. Lorundrostat has the lowest $C_{max}$ at a single dose of 10 mg, but its $AUC_{0\text{-}24}$ is higher than that of both Dexfadrostat and LCI699 at the same dosage, and the drug is eliminated slowly enough to achieve a certain blood concentration at steady state.

TABLE 2 ADME parameters of five ASIs predicted by ML before calibration.

| Symbol | Parameters (Unit) | Baxdrostat | BI689648 | Lorundrostat | Dexfadrostat | LCI699 |
|---|---|---|---|---|---|---|
| MW | molecular weight (g/mol) | 363.50 | 298.36 | 451.6 | 223.27 | 227.24 |
| $f_{up}$ | unbound fraction to plasma protein | 0.26[a] | 0.18 | 0.11 | 0.18 | 0.20 |
| bpr | blood-to-plasma ratio | 0.96 | 1.04 | 0.66 | 0.74 | 0.77 |
| gi_ka | GI absorption rate constant ($h^{-1}$) | 0.96 | 0.73 | 0.36 | 0.86 | 1.63 |
| $CL_{app}$ | clearance (L/h) | 14.83 | 14.32 | 39.36 | 71.11 | 95.05 |
| $V_{ss}$_perKg | $V_{ss}$ (L/kg) | 1.37 | 1.29 | 1.54 | 1.67 | 1.58 |
| kp_bone | bone: plasma | 2.55 | 0.24 | 0.33 | 1.21 | 0.73 |
| kp_brain | brain: plasma | 45.07 | 0.22 | 0.29 | 1.03 | 0.63 |
| kp_adipose | adipose: plasma | 18.05 | 1.29 | 2.20 | 11.88 | 6.58 |
| kp_heart | heart: plasma | 7.31 | 0.37 | 0.46 | 1.55 | 0.97 |
| kp_kidney | kidney: plasma | 7.12 | 0.28 | 0.30 | 0.81 | 0.55 |
| kp_gut | gut: plasma | 9.81 | 0.30 | 0.36 | 0.98 | 0.64 |
| kp_liver | liver: plasma | 4.75 | 0.23 | 0.26 | 0.76 | 0.50 |
| kp_lung | Lung: plasma | 9.41 | 0.26 | 0.30 | 0.31 | 0.29 |
| kp_muscle | muscle: plasma | 8.02 | 0.13 | 0.19 | 0.34 | 0.25 |
| kp_skin | skin: plasma | 37.69 | 0.39 | 0.46 | 1.05 | 0.73 |
| kp_spleen | spleen: plasma | 5.39 | 0.19 | 0.22 | 0.41 | 0.31 |
| Kp_scaler | Kp scaler | 0.16 | 3.75 | 3.33 | 0.91 | 1.46 |

[a]The $f_{up}$ of Baxdrostat is from the literature.

TABLE 3 Important PK parameters of 2.5 mg Baxdrostat simulated before and after calibration, and observed ones.

| PK parameters | Simulated before calibration | Observed[a] | Simulated after calibration |
|---|---|---|---|
| $AUC_{0\text{-}24}$ (ng*hr/mL) | 157.25 | 365.79 | 396.55 |
| $C_{max}$ (ng/mL) | 18.99 | 28.09 | 23.97 |
| $T_{1/2}$ (hr) | 6.10 | 28.37 | 21.80 |
| $T_{max}$ (hr) | 1.20 | 3.00 | 1.80 |

[a]The observed data are from the literature (Freeman et al., 2023).

## 3.3 Simulation of PD for all five compounds

Clinical PD endpoints for ASIs are not limited to the change in seated mean systolic blood pressure from baseline to 8 weeks of treatment. For model construction, with limited *in vitro* clinical trial data and inconsistent PD endpoint metrics, the choice of $IC_{50}$ as an input to the PD model allows for a direct comparison of the inhibitory effects of different compounds on AS and 11β-hydroxylase. Therefore, selective inhibition of AS without affecting 11β-hydroxylase is an observable indicator for PD evaluation in our study. By comparing the trend of the inhibition rate of a compound on AS and 11β-hydroxylase with dosage change, we can obtain the dosage range of the compound reaching the optimal inhibition rate and can compare different compounds at the same dosage or with the same inhibition effect. This analysis is limited for not fully reflecting the PD endpoints of clinical trials, but it can provide ideas for dosage recommendation and comparison of the efficacy of different compounds. The $E_{max}$ model was used to predict the PD of all five compounds based on plasma free drug concentrations, and the $IC_{50}$ was used as an input parameter (Table 6). For Baxdrostat, the $IC_{50}$ is from the clinical data (Bogman et al., 2017). For the other drugs, the $IC_{50}$ data are from monkey adrenal gland homogenate (Weldon et al., 2016; Laffin et al., 2023). The enzyme inhibition rates of single and multiple doses predicted for all the compounds are shown in Figure 7.

It can be seen that the inhibition of the enzymes increased in a dosage-dependent manner. As can be seen from the multiple doses plot, when the steady state was reached, Baxdrostat at a dosage of 3 mg showed a 65% inhibition of AS. When the dosage was 10 mg, the inhibition rate of AS reached 85%, the inhibition of 11β-hydroxylase began to increase significantly, and the

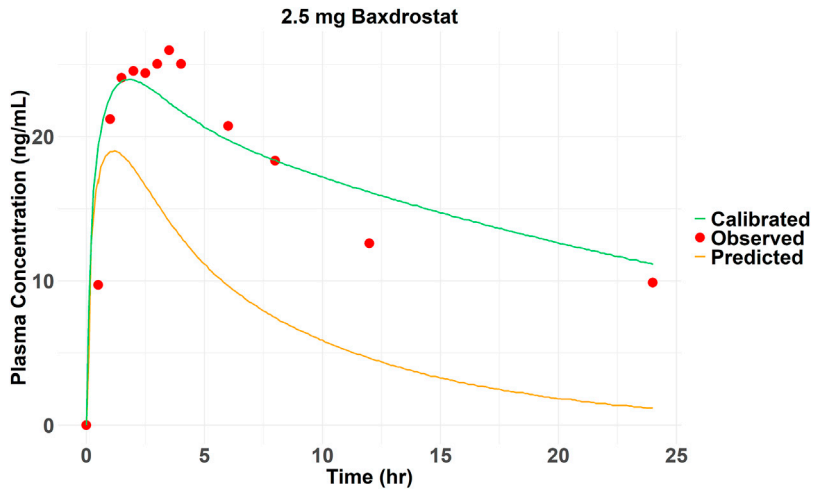


FIGURE 3
Observed and predicted (before and after calibration) plasma drug concentrations of 2.5 mg Baxdrostat over time.

TABLE 4 $CL_{app}$ and Kp_scaler of five ASIs after calibration.

| Symbol | Baxdrostat | BI689648 | Lorundrostat | Dexfadrostat | LCI699 |
|---|---|---|---|---|---|
| $CL_{app}$ | 3.15 | 3.05 | 8.37 | 15.13 | 20.22 |
| Kp_scaler | 0.14 | 3.19 | 2.83 | 0.78 | 1.24 |

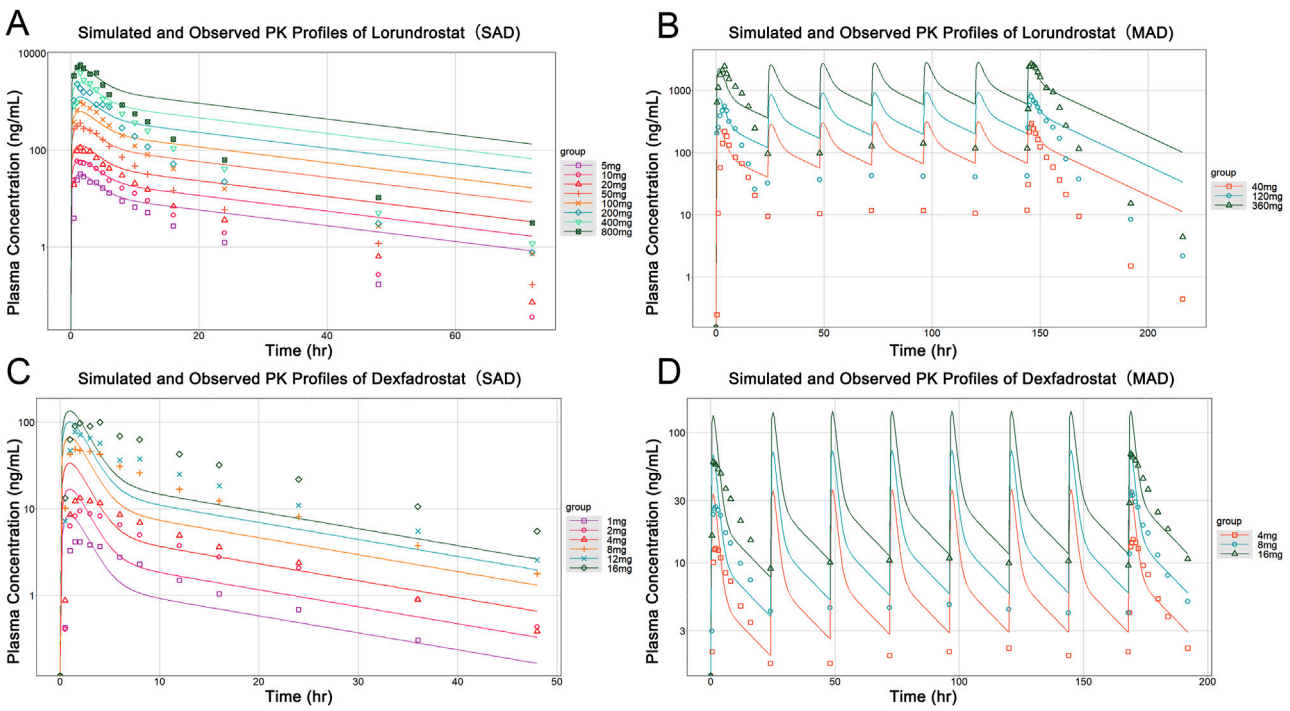


FIGURE 4
Observed versus predicted PK profiles of Lorundrostat and Dexfadrostat at different dosages. **(A)** Simulated and observed profiles for a single dose of Lorundrostat (5, 10, 20, 50, 100, 200, 400, 800 mg). **(B)** Simulated and observed profiles of Lorundrostat at multiple doses (40 mg, 120 mg, 360 mg). **(C)** Simulated and observed profiles for a single dose of Dexfadrostat (1 mg, 2 mg, 4 mg, 8 mg, 12 mg, 16 mg). **(D)** Simulated and observed profiles of Dexfadrostat at multiple doses (4 mg, 8 mg, 16 mg).

TABLE 5 Ratio of predicted to observed $C_{max}$, $T_{max}$, $AUC_{0-24}$ values for three ASIs at different dosages and dosing modules.

| Name | Dosage (mg) | Dosing module | Ratio | | |
|---|---|---|---|---|---|
| | | | $RC_{max}$ | $RT_{max}$ | $RAUC_{0-24}$ |
| Baxdrostat | 0.5 | SAD | 1.01 | 0.90 | 1.04 |
| Baxdrostat | 0.5 | MAD | 0.97 | 0.50 | 1.00 |
| Dexfadrostat | 1 | SAD | 1.98 | 0.68 | 0.88 |
| Dexfadrostat | 2 | SAD | 1.73 | 0.68 | 0.74 |
| Dexfadrostat | 4 | SAD | 2.54 | 0.69 | 1.11 |
| Dexfadrostat | 8 | SAD | 1.35 | 1.09 | 0.61 |
| Dexfadrostat | 12 | SAD | 1.28 | 1.09 | 0.66 |
| Dexfadrostat | 16 | SAD | 1.37 | 0.68 | 0.54 |
| Dexfadrostat | 4 | MAD | 2.40 | 0.50 | 1.26 |
| Dexfadrostat | 8 | MAD | 2.11 | 0.73 | 1.20 |
| Dexfadrostat | 16 | MAD | 2.14 | 1.31 | 1.11 |
| Lorundrostat | 5 | SAD | 0.76 | 0.93 | 0.73 |
| Lorundrostat | 10 | SAD | 1.08 | 0.93 | 0.88 |
| Lorundrostat | 20 | SAD | 1.17 | 0.93 | 1.50 |
| Lorundrostat | 50 | SAD | 0.84 | 0.94 | 1.28 |
| Lorundrostat | 100 | SAD | 0.61 | 0.94 | 1.09 |
| Lorundrostat | 200 | SAD | 0.54 | 1.40 | 1.08 |
| Lorundrostat | 400 | SAD | 0.66 | 1.40 | 1.31 |
| Lorundrostat | 800 | SAD | 0.86 | 0.94 | 1.55 |
| Lorundrostat | 40 | MAD | 1.12 | 0.77 | 2.00 |
| Lorundrostat | 120 | MAD | 1.26 | 1.07 | 1.72 |
| Lorundrostat | 360 | MAD | 1.02 | 1.10 | 1.35 |

TABLE 6 $IC_{50}$ and selective index of five ASIs for 11β-hydroxylase and aldosterone synthase for PD prediction.

| Name | $IC_{50}$ (nmol/L) and SI | | | | |
|---|---|---|---|---|---|
| | LCI699 (Weldon et al., 2016) | Dexfadrostat (Weldon et al., 2016) | BI 689648 (Weldon et al., 2016) | Baxdrostat (Bogman et al., 2017) | Lorundrostat (Laffin et al., 2023; Mineralys Therapeutics, 2023; Shimizu et al., 2024) |
| 11β-hydroxylase | 77 | 94 | 310 | 1,310 | 475 |
| Aldosterone synthase | 10 | 2.5 | 2.1 | 13 | 1.27 |
| SI[a] | 7.7 | 38 | 149 | 100 | 374 |

[a]SI, is defined as the ratio of $IC_{50}$ for 11β-hydroxylase over $IC_{50}$ for aldosterone synthase.

selectivity of the compound gradually decreased. Therefore, the optimal dosage of Baxdrostat predicted in this study is 10 mg, with an AS inhibition rate of 85%. In the clinical trials, after the healthy subjects received a single increasing dosage of Baxdrostat, the plasma aldosterone decreased in a dosage-dependent manner with the maximum effect reached at 10 mg (Bogman et al., 2017). The predicted best inhibitory effect of Baxdrostat was also reached at 10 mg, with a strong inhibition of AS and weak inhibition of 11β-hydroxylase, echoing the clinical trial data. When BI689648 was administered at a dosage of 3 mg, the inhibition of AS reached 90%, at which point the inhibition of 11β-hydroxylase began to increase and the side effects started to

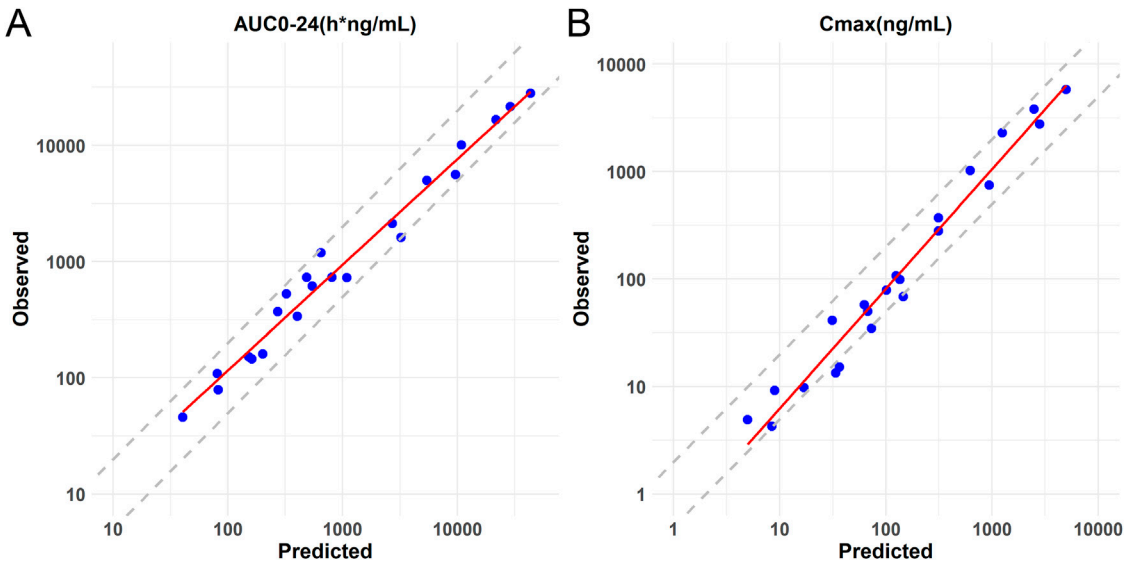


FIGURE 5
Logarithmic coordinate plots of predicted versus observed values of $AUC_{0\text{-}24}$ and $C_{max}$ for Baxdrostat, Dexfadrostat and Lorundrostat. The solid line represents the linear regression fit of the data. **(A)** Predicted versus observed $AUC_{0\text{-}24}$ with 2-fold and 0.5-fold deviation lines. **(B)** Predicted versus observed $C_{max}$ with 2-fold and 0.5-fold deviation lines.

become apparent. Therefore, the optimal dosage of BI689648 is 3 mg, achieving an AS inhibition rate of 90%. At a dosage of 3 mg, the inhibitory effect of Baxdrostat on AS was only 65%, which was lower than that of BI689648 at the same dosage. When Lorundrost was administered at a dosage of 3 mg, the inhibition of AS reached 75%, which was slightly lower than that of BI689648 at 3 mg, and was comparable to the effect of BI689648 at 1 mg. As the dosage increased to 12.5 mg, the inhibition of AS reached 90%, at that point the inhibition of 11β-hydroxylase began to increase. The inhibition at this point was comparable to that of BI689648 at 3 mg. Therefore, the optimal dosage of Lorundrost in our predicted PD is 12.5 mg, and the inhibition rate of AS can reach 90%. With dosage increasing, the inhibition of 11β-hydroxylase by Baxdrostat, Lorundrost, and BI689648 becomes more pronounced. For Dexfadrostat and LCI699, the inhibition of AS and 11β-hydroxylase are very close to each other, thus neither drug is very selective.

## 4 Discussion

In this study, we used all available data of Baxdrostat to build the best possible general AI-PBPK model for ASIs and used clinical PK data for correction. Data from clinical PK trials of Dexfadrostat and Lorundrost were used in subsequent external validation to assess the model's performance and generalizability across clusters. This validation process allowed for an assessment of the model's ability to simulate biological processes, identify biases, and refine its predictive capabilities, ensuring credibility and reliability for real-world applications (Collins et al., 2024). The validation component is therefore of great value in improving the goodness of fit of the model. The results of model validation showed that the ratios of most predicted-to-observed $AUC_{0\text{-}24}$ and $C_{max}$ values were in the range of 1/2-fold–2-fold, reflecting the validity of the model in simulating PK behaviors. Yet, four $C_{max}$ ratio data fell outside of this range, suggesting deficiencies in parameter estimation. And in the absence of sufficient clinical trial data to calibrate the model, the predictions may be biased due to the lack of calibration conditions (Huang et al., 2002).

PK prediction of all five compounds at the same dosage showed that Baxdrostat, BI689648, Lorundrostat had higher $AUC_{0\text{-}24}$ than LCI699, and the highest drug exposure was found for BI689648, followed by Baxdrostat, Dexfadrostat, and LCI699. The $AUC_{0\text{-}24}$ of Lorundrostat was intermediate between that of Baxdrostat and Dexfadrostat for a single dose of 10 mg and multiple doses of 3 mg. The PD results corresponding to PK showed that when the inhibition rate of 11β-hydroxylase did not start to fluctuate, the compound with the highest selectivity for AS and 11β-hydroxylase was Lorundrostat at 3 mg, followed by BI689648 at 1 mg, and Baxdrostat at 3 mg, and their inhibition of AS could reach 80%, 75% and 65%, respectively. This trend was consistent with the *in vitro* observational data (Lorundrostat SI: 374, BI689648 SI: 149, Baxdrostat SI: 100, Dexfadrostat SI: 38) (Weldon et al., 2016; Bogman et al., 2017; Laffin et al., 2023; Shimizu et al., 2024). LCI699 at a dosage of 0.5 mg exhibited a potent inhibition of 11β-hydroxylase activity, further substantiating the efficacy of LCI699 as a 11β-hydroxylase inhibitor (LCI699 SI: 7.7) (Weldon et al., 2016). The predicted PD trend matched the clinically observed one, validating the capacity of the model in translational research. Thus, PD prediction for more similar ASIs based on their structural formulae could be performed to assess their potential (Mehić, 2011). The pivotal Phase III clinical trial of Lorundrostat (Launch-HTN, NCT06153693) successfully met its primary endpoint, resulting in a 16.9 mmHg reduction in systolic blood pressure after treatment with Lorundrostat at 50 mg, in contrast to a placebo-adjusted reduction

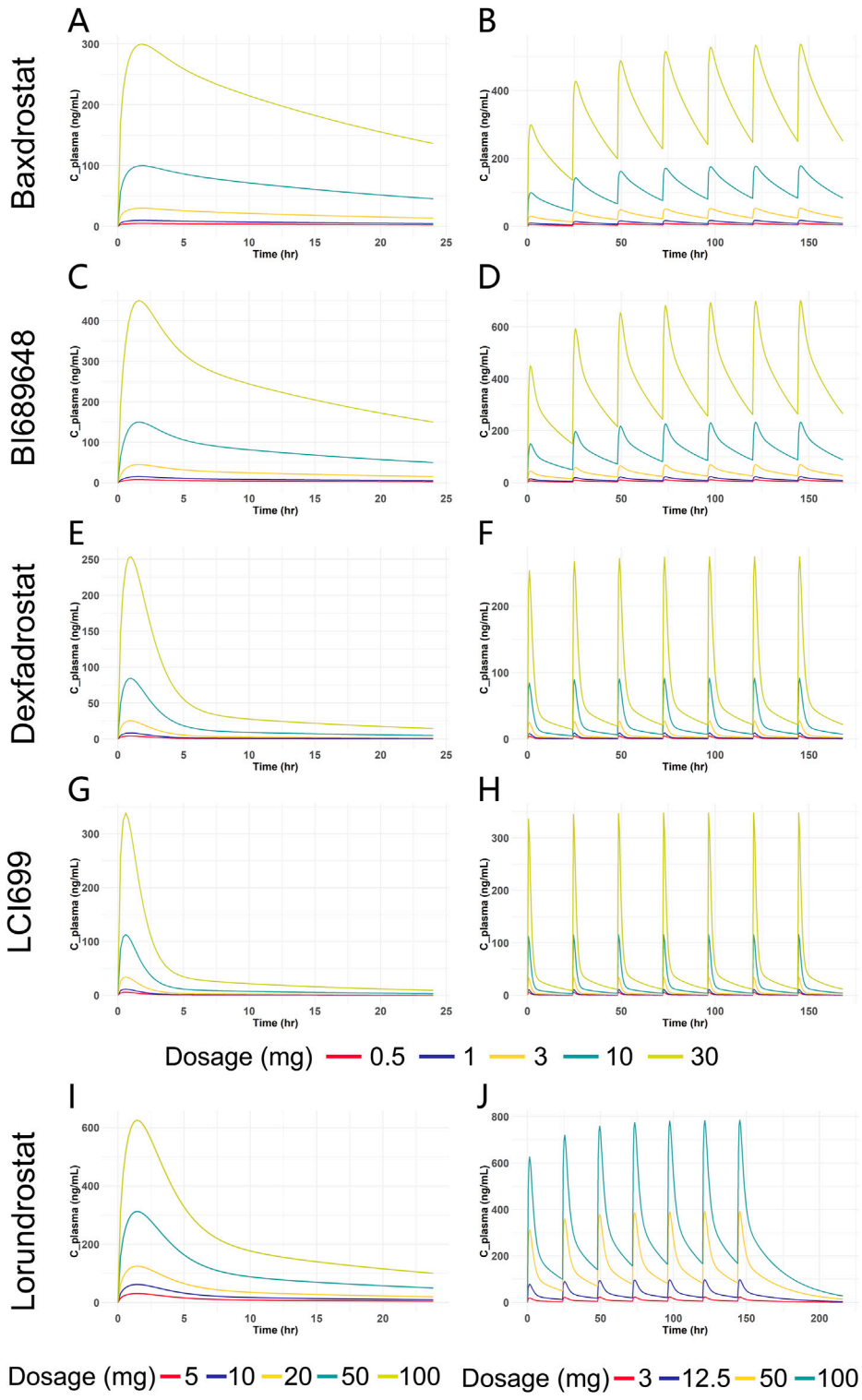


FIGURE 6
Predicted plasma drug concentration versus time curves for five ASIs at different dosages. **(A)** Blood drug concentration-time curves of Baxdrostat at SAD. **(B)** Blood drug concentration-time curves of Baxdrostat at MAD. **(C)** Blood drug concentration-time curves of BI689648 at SAD. **(D)** Blood drug concentration-time curves of BI689648 at MAD. **(E)** Blood drug concentration-time curves of Dexfadrostat at SAD. **(F)** Blood drug concentration-time curves of Dexfadrostat at MAD. **(G)** Blood drug concentration-time curves of LCI699 at SAD. **(H)** Blood drug concentration-time curves of LCI699 at MAD. **(I)** Blood drug concentration-time curves of Lorundrostat at SAD. **(J)** Blood drug concentration-time curves of Lorundrostat at MAD.

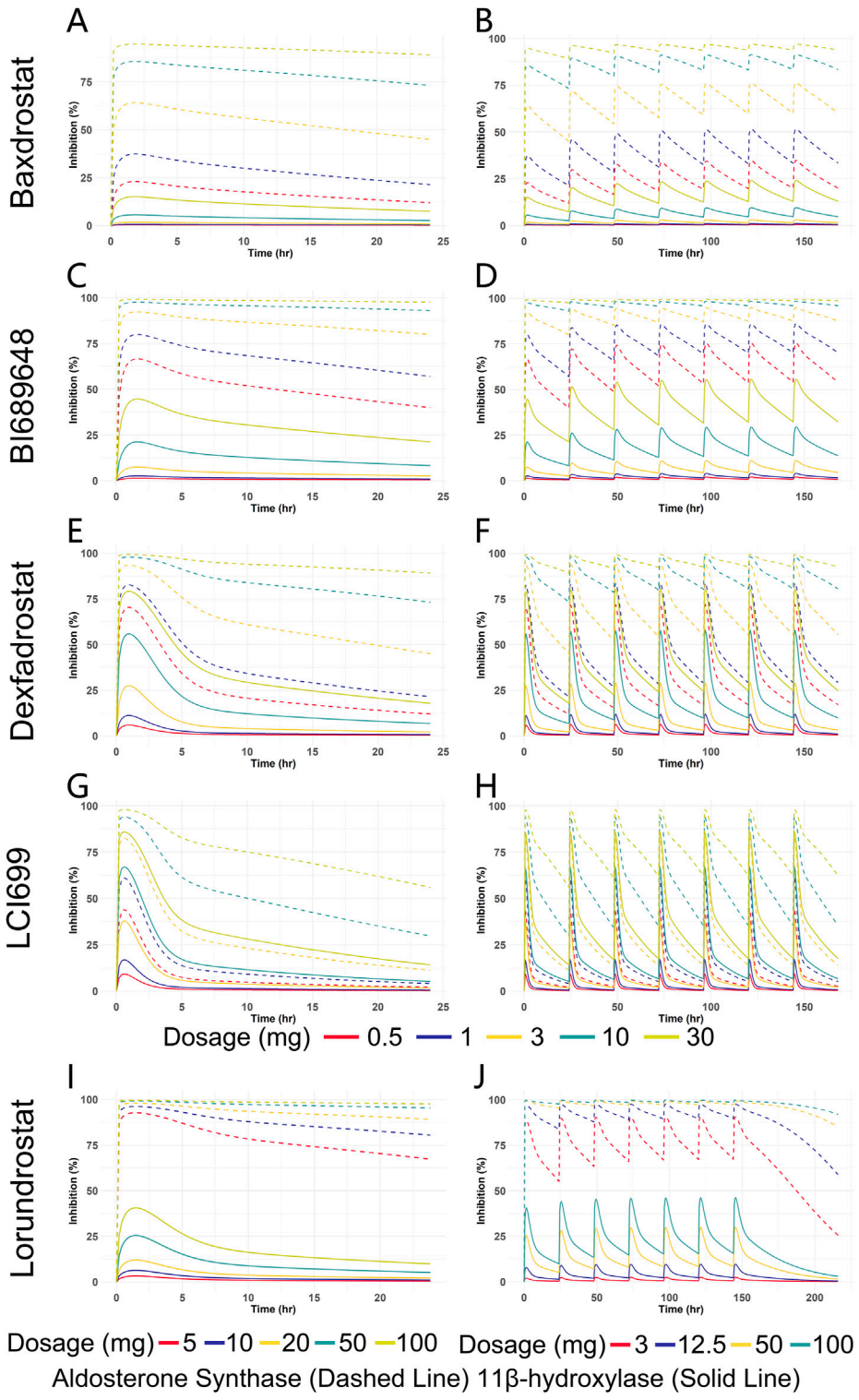


FIGURE 7
Predicted inhibition rate versus time curves for five ASIs at different dosages. **(A)** Enzyme inhibition over time for Baxdrostat at SAD. **(B)** Enzyme inhibition over time for Baxdrostat at MAD. **(C)** Enzyme inhibition over time for BI689648 at SAD. **(D)** Enzyme inhibition over time for BI689648 at MAD. **(E)** Enzyme inhibition over time for Dexfadrostat at SAD. **(F)** Enzyme inhibition over time for Dexfadrostat at MAD. **(G)** Enzyme inhibition over time for LCI699 at SAD. **(H)** Enzyme inhibition over time for LCI699 at MAD. **(I)** Enzyme inhibition over time for Lorundrostat at SAD. **(J)** Enzyme inhibition over time for Lorundrostat at MAD.

of 9.1 mmHg ($p < 0.0001$), as shown by automated office blood pressure measurement at week 6. Additionally, the trial met a predefined endpoint at the end of treatment (week 12), where Lorundrostat at 50 mg led to a 19.0 mmHg reduction in systolic blood pressure, against an 11.7 mmHg placebo-adjusted reduction ($p < 0.0001$). This is of great significance for the treatment of Uncontrolled or Resistant Hypertension with ASIs. It demonstrates to some extent the feasibility of our PD prediction. Thus, in the preclinical stage, PD prediction based only on limited data and compounds structural formulae can provide ideas for dosage recommendations and efficacy comparisons of different compounds, and such predictive models are of great value.

Nevertheless, inconsistence existed between certain predicted and observed parameters. Results of a randomized, placebo-controlled, dosage-varied trial in adults with uncontrolled hypertension taking two or more antihypertensive medicines (Laffin et al., 2023) showed that Lorundrostat resulted in a reduction in serum aldosterone at all dosages, and there were only small increases in serum cortisol. In our predicted PD, the inhibition rate of 11β-hydroxylase became apparent for Lorundrostat at 12.5 mg, which showed some differences from the results in human clinical trials. This may be due to that the gene expression of CYP11B2 and CYP11B1 in the adrenal gland is regulated by epigenetic modification, which contributes to autonomous aldosterone and cortisol synthesis (Takeda et al., 2023). In addition, the simulated inhibition rates did not take into account the effect of differences in drug metabolism *in vivo*, which involves highly complex cooperation between drug transporter proteins and drug-conjugating and metabolizing enzymes, as well as targeted programs of gene activation and proteasomal degradation pathways. Moreover, drug transport and metabolism in the intestine and liver mediate the systemic delivery of therapeutic compounds (Staudinger, 2013). In addition, using $IC_{50}$ from different species as inputs to the $E_{max}$ model and drawing conclusions based on predicted PD may be flawed and error-prone for predicting clinical effectiveness. Cross-species and in vitro-in vivo extrapolations require consideration of species-specific physiology, plasma protein binding, enzyme and transport kinetics, and tissue-specific gene expression profiles. Comprehensive considerations can increase the accuracy of cross-species and in vitro-in vivo extrapolations (Thiel et al., 2015).

Overall, for simulation of an ASI's PD with the AI-PBPK model, the bias in results predicted by the model arises primarily from two factors: (1) the inherent imprecision of machine learning in predicting compound-specific parameters, influenced by the data sources and prediction methods employed, and (2) the combination of ML prediction bias with PBPK model bias, which amplifies inaccuracies in PK data and subsequent PD modeling. These biases are inherent limitations of current models, which hinder the models from fully accounting for variations across individuals, races, and disease populations (Cross et al., 2024). In 2024, Chen et al. systematically analyzed the main factors affecting prediction accuracy through a model-driven pharmacogenetic-pharmacodynamic (PG/PD) exploration with a machine learning approach (Chen et al., 2024). Approaches proposed by them to reduce bias include sensitivity analyses to identify key parameters and improve the relevance of data collection; the use of large-scale biomarker data to improve PK/PD associations; and the use of multiple machine-learning algorithms for cross-validation to improve the model's robustness (Chen et al., 2024).

From the perspective of model generalizability, the AI-PBPK model can predict drug-specific parameters and PK exposure based solely on a compound's molecular structure. In a previous work on proton pump inhibitors, the model validation showed a Pearson correlation coefficient (r) between 0.84 and 0.89, with consistent trends between predicted and observed PK data (Wu et al., 2024). In the current case of ASIs, the model's fit to $AUC_{0\text{-}24}$ and $C_{max}$ was evaluated, both showing a coefficient of determination greater than 0.95. From the existing work on ASIs, there is considerable room for improvement in predicting certain drug-specific parameters, such as clearance. Overall, this study provides a method for predicting a compound's PK/PD based on its structural formula at the drug discovery stage and presents an AI-PBPK/PD model for ASIs, which can predict the PK characteristics of similar ASIs in the human body, analyze the dose-exposure and exposure-effect, *etc.*, providing a reference for subsequent compound screening and clinical research.

## 5 Conclusion

The AI-PBPK model was employed to predict the PK profiles of five aldosterone synthase inhibitors, and the inhibition of aldosterone synthase and 11β-hydroxylase by the five compounds was predicted using a PD model based on their free blood concentrations. It is realized that a compound's PK/PD in the human body can be obtained through predictions based on its structural formula at the drug discovery stage. This can accelerate ASIs screening, avoiding the extensive trial and error process. Yet, there is still considerable room for improvement in model fitting. We will carry out more case studies to further prove the model's effectiveness and continuously optimize the model to improve its overall prediction accuracy. With further improvement, our AI-PBPK model on the $B^2O$ simulation platform shall have great potential to predict the therapeutic effects of drug candidates at the early stages of drug discovery.

## Data availability statement

The original contributions presented in the study are included in the article/Supplementary Material, further inquiries can be directed to the corresponding author.

## Author contributions

MZ: Data curation, Investigation, Visualization, Writing – original draft, Writing – review and editing. KW: Conceptualization, Data curation, Formal Analysis, Methodology, Software, Validation, Writing – review and editing. SL: Writing – review and editing. XJ: Data curation,

Writing – review and editing. BL: Conceptualization, Project administration, Writing – review and editing.

## Funding

The author(s) declare that no financial support was received for the research and/or publication of this article.

## Acknowledgments

We thank Yinghan Pharmaceutical Technology (Shanghai) Co., Ltd. for supporting this study.

## Conflict of interest

Author KW was employed by Yinghan Pharmaceutical Technology (Shanghai) Co., Ltd.

The remaining authors declare that the research was conducted in the absence of any commercial or financial relationships that could be construed as a potential conflict of interest.

## Generative AI statement

The author(s) declare that no Generative AI was used in the creation of this manuscript.

## Publisher's note



## Supplementary material

The Supplementary Material for this article can be found online at: https://www.frontiersin.org/articles/10.3389/fphar.2025.1578117/full#supplementary-material

## References

Andersen, K., Hartman, D., Peppard, T., Hermann, D., Van Ess, P., Lefkowitz, M., et al. (2012). The effects of aldosterone synthase inhibition on aldosterone and cortisol in patients with hypertension: a phase II, randomized, double-blind, placebo-controlled, multicenter study. *J. Clin. Hypertens. (Greenwich)* 14 (9), 580–587. doi:10.1111/j.1751-7176.2012.00667.x

Arafat, M., Sarfraz, M., and AbuRuz, S. J. P. (2021). Development and *in vitro* evaluation of controlled release Viagra® containing Poloxamer-188 using Gastroplus™ PBPK modeling software for *in vivo* predictions and pharmacokinetic assessments. *Pharm. Basel, Switz.* 14 (5), 479. doi:10.3390/ph14050479

Awosika, A., Cho, Y., Bose, U., Omole, A. E., and Adabanya, U. (2023). Evaluating phase II results of Baxdrostat, an aldosterone synthase inhibitor for hypertension. *Expert Opin. Investig. Drugs* 32 (11), 985–995. doi:10.1080/13543784.2023.2276755

Azzam, K. A. (2023). SwissADME and pkCSM webservers predictors: an integrated online platform for accurate and comprehensive predictions for *in silico* ADME/T properties of artemisinin and its derivatives. *Kompleksnoe Ispolzovanie Mineralnogo Syra= Complex use mineral Resour.* 325 (2), 14–21. doi:10.31643/2023/6445.13

Balhara, A., Kale, S., and Singh, S. (2022). "Physiologically based parmacokinetic (PBPK) modelling," in *Computer aided pharmaceutics and drug delivery: an application guide for students and researchers of pharmaceutical sciences*. Editor V. Saharan (Singapore: Springer Nature Singapore), 255–284.

Bogman, K., Schwab, D., Delporte, M. L., Palermo, G., Amrein, K., Mohr, S., et al. (2017). Preclinical and early clinical profile of a highly selective and potent oral inhibitor of aldosterone synthase (CYP11B2). *Hypertension* 69 (1), 189–196. doi:10.1161/HYPERTENSIONAHA.116.07716

Chen, E., Bondi, R., and Michalski, P. (2021). Model-based Target Pharmacology Assessment (mTPA): an approach using PBPK/PD modeling and machine learning to design medicinal chemistry and DMPK strategies in early drug discovery. *J. Med. Chem.* 64 (6), 3185–3196. doi:10.1021/acs.jmedchem.0c02033

Chen, E. P., Dutta, S., Ho, M.-H., and DeMartino, M. P. (2024). Model-based virtual PK/PD exploration and machine learning approach to define PK drivers in early drug discovery. *J. Med. Chem.* 67 (5), 3727–3740. doi:10.1021/acs.jmedchem.3c02169

Chou, W., and Lin, Z. (2023). Machine learning and artificial intelligence in physiologically based pharmacokinetic modeling. *Toxicol. Sci.* 191 (1), 1–14. doi:10.1093/toxsci/kfac101

Collins, G. S., Dhiman, P., Ma, J., Schlussel, M. M., Archer, L., Van Calster, B., et al. (2024). Evaluation of clinical prediction models (part 1): from development to external validation. *BMJ Clin. Res. ed.* 384, e074819. doi:10.1136/bmj-2023-074819

Cross, J. L., Choma, M. A., and Onofrey, J. A. (2024). Bias in medical AI: implications for clinical decision-making. *PLOS Digit. Health* 3 (11), e0000651. doi:10.1371/journal.pdig.0000651

Daina, A., Michielin, O., and Zoete, V. (2017). SwissADME: a free web tool to evaluate pharmacokinetics, drug-likeness and medicinal chemistry friendliness of small molecules. *Sci. Rep.* 7, 42717. doi:10.1038/srep42717

Dang, N. L., Matlock, M. K., Hughes, T. B., and Swamidass, S. J. (2020). The metabolic rainbow: deep learning phase I metabolism in five colors. *J. Chem. Inf. Model.* 60 (3), 1146–1164. doi:10.1021/acs.jcim.9b00836

Dormoy, A., Haissaguerre, M., Vitellius, G., Do Cao, C., Geslot, A., Drui, D., et al. (2023). Efficacy and safety of Osilodrostat in paraneoplastic cushing syndrome: a real-world multicenter study in France. *J. Clin. Endocrinol. Metab.* 108 (6), 1475–1487. doi:10.1210/clinem/dgac691

Ezuruike, U., Zhang, M., Pansari, A., De Sousa Mendes, M., Pan, X., Neuhoff, S., et al. (2022). Guide to development of compound files for PBPK modeling in the Simcyp population-based simulator. *CPT pharmacometrics and Syst. Pharmacol.* 11 (7), 805–821. doi:10.1002/psp4.12791

Freeman, M., Bond, M., Murphy, B., Hui, J., and Isaacsohn, J. (2023). Results from a phase 1, randomized, double-blind, multiple ascending dose study characterizing the pharmacokinetics and demonstrating the safety and selectivity of the aldosterone synthase inhibitor baxdrostat in healthy volunteers. *Hypertens. Res.* 46 (1), 108–118. doi:10.1038/s41440-022-01070-4

Freitas, A., Limbu, K., and Ghafourian, T. (2015). Predicting volume of distribution with decision tree-based regression methods using predicted tissue:plasma partition coefficients. *J. Cheminform* 7 (1), 6. doi:10.1186/s13321-015-0054-x

Fu, L., Shi, S., Yi, J., Wang, N., He, Y., Wu, Z., et al. (2024). ADMETlab 3.0: an updated comprehensive online ADMET prediction platform enhanced with broader coverage, improved performance, API functionality and decision support. *Nucleic Acids Res.* 52 (W1), W422–w431. doi:10.1093/nar/gkae236

Gilmer, J., Schoenholz, S. S., Riley, P. F., Vinyals, O., and Dahl, G. E. (2017). "Neural message passing for quantum chemistry," in *Proceedings of the 34th international conference on machine learning - volume 70* (Sydney, NSW, Australia: JMLR.org).

Haid, R. T. U., and Reichel, A. (2024). Transforming the discovery of targeted protein degraders: the translational power of predictive PK/PD modeling. *Clin. Pharmacol. Ther.* 116 (3), 770–781. doi:10.1002/cpt.3273

Hargovan, M., and Ferro, A. (2014). Aldosterone synthase inhibitors in hypertension: current status and future possibilities. *JRSM Cardiovasc Dis.* 3, 2048004014522440. doi:10.1177/2048004014522440

Helander, H., and Fändriks, L. (2014). Surface area of the digestive tract – revisited. *Scand. J. Gastroenterol.* 49 (6), 681–689. doi:10.3109/00365521.2014.898326

Huang, J., Brennan, D., Sattler, L., Alderman, J., Lane, B., and O'Mathuna, C. (2002). A comparison of calibration methods based on calibration data size and robustness. *Chemom. Intelligent Laboratory Syst.* 62 (1), 25–35. doi:10.1016/S0169-7439(01)00211-8

Huang, K., Fu, T., Gao, W., Zhao, Y., Roohani, Y., Leskovec, J., et al. (2021). Therapeutics data commons: machine learning datasets and tasks for drug discovery and development. *arXiv e-prints, arXiv:2102.09548*. doi:10.48550/arXiv.2102.09548

Jiménez-Luna, J., Skalic, M., Weskamp, N., and Schneider, G. (2021). Coloring molecules with explainable artificial intelligence for preclinical relevance assessment. *J. Chem. Inf. Model* 61 (3), 1083–1094. doi:10.1021/acs.jcim.0c01344

Laffin, L., Rodman, D., Luther, J., Vaidya, A., Weir, M., Rajicic, N., et al. (2023). Aldosterone synthase inhibition with Lorundrostat for uncontrolled hypertension: the target-HTN randomized clinical trial. *JAMA* 330 (12), 1140–1150. doi:10.1001/jama.2023.16029

Li, Y., Wang, Z., Li, Y., Du, J., Gao, X., Li, Y., et al. (2024). A combination of machine learning and PBPK modeling approach for pharmacokinetics prediction of small molecules in humans. *Pharm. Res.* 41 (7), 1369–1379. doi:10.1007/s11095-024-03725-y

Macdougall, J. (2006). "Analysis of dose–response studies—Emax model," in *Dose finding in drug development*. Editor N. Ting (New York, NY: Springer), 127–145.

Mamada, H., Iwamoto, K., Nomura, Y., and Uesawa, Y. (2021). Predicting blood-to-plasma concentration ratios of drugs from chemical structures and volumes of distribution in humans. *Mol. Divers* 25 (3), 1261–1270. doi:10.1007/s11030-021-10186-7

Marques, L., Costa, B., Pereira, M., Silva, A., Santos, J., Saldanha, L., et al. (2024). Advancing precision medicine: a review of innovative *in silico* approaches for drug development, clinical pharmacology and personalized healthcare. *Pharmaceutics* 16 (3), 332. doi:10.3390/pharmaceutics16030332

Mazzieri, A., Timio, F., Patera, F., Trepiccione, F., Bonomini, M., and Reboldi, G. (2024). Aldosterone synthase inhibitors for cardiorenal protection: ready for prime time? *Kidney Blood Press Res.* 49 (1), 1041–1056. doi:10.1159/000542621

Mehić, B. (2011). Translational research in medicine. *Bosn. J. Basic Med. Sci.* 11 (2), 73. doi:10.17305/bjbms.2011.2583

Miguel, C., Reinhold, K., and Myeong-Chan, C. (2024). Diagnosis and management of resistant hypertension. *Heart* 385, e079108. doi:10.1136/bmj-2023-079108

Mineralys Therapeutics, I. (2023). Annual report (form 10-K). Available online at: https://ir.mineralystx.com/sec-filings/all-sec-filings/content/0001628280-24-012358/0001628280-24-012358.pdf.

Mulatero, P., Groessl, M., Vogt, B., Schumacher, C., Steele, R., Brooks, A., et al. (2023). CYP11B2 inhibitor dexfadrostat phosphate suppresses the aldosterone-to-renin ratio, an indicator of sodium retention, in healthy volunteers. *Br. J. Clin. Pharmacol.* 89 (8), 2483–2496. doi:10.1111/bcp.15713

Nishimoto, K., Ogishima, T., Sugiura, Y., Suematsu, M., and Mukai, K. (2023). Pathology and gene mutations of aldosterone-producing lesions. *Endocr. J.* 70 (12), 1113–1122. doi:10.1507/endocrj.EJ22-0492

Papillon, J., Adams, C., Hu, Q., Lou, C., Singh, A., Zhang, C., et al. (2015). Structure-activity relationships, pharmacokinetics, and *in vivo* activity of CYP11B2 and CYP11B1 inhibitors. *J. Med. Chem.* 58 (11), 4749–4770. doi:10.1021/acs.jmedchem.5b00407

Peters, S. (2021). "Applications of physiologically based pharmacokinetic models integrated with drug effect models (PBPK/PD)," in *Physiologically based pharmacokinetic (PBPK) modeling and simulations*. Editor S. Peters (Hoboken: Wiley-Blackwell), 353–374.

Rigel, D., Fu, F., Beil, M., Hu, C., Liang, G., and Jeng, A. (2010). Pharmacodynamic and pharmacokinetic characterization of the aldosterone synthase inhibitor FAD286 in two rodent models of hyperaldosteronism: comparison with the 11beta-hydroxylase inhibitor metyrapone. *J. Pharmacol. Exp. Ther.* 334 (1), 232–243. doi:10.1124/jpet.110.167148

Shimizu, H., Tortorici, M., Ohta, Y., Ogawa, K., Rahman, S., Fujii, A., et al. (2024). First-in-human study evaluating safety, pharmacokinetics, and pharmacodynamics of lorundrostat, a novel and highly selective aldosterone synthase inhibitor. *Clin. Transl. Sci.* 17 (8), e70000. doi:10.1111/cts.70000

Staudinger, J. L. (2013). Disease, drug metabolism, and transporter interactions. *Pharm. Res.* 30 (9), 2171–2173. doi:10.1007/s11095-013-1129-x

Swanson, K., Walther, P., Leitz, J., Mukherjee, S., Wu, J. C., Shivnaraine, R. V., et al. (2023). ADMET-AI: a machine learning ADMET platform for evaluation of large-scale chemical libraries. *bioRxiv, 2023.12.28.573531*. doi:10.1101/2023.12.28.573531

Takeda, Y., Demura, M., Kometani, M., Karashima, S., Yoneda, T., and Takeda, Y. (2023). Molecular and epigenetic control of aldosterone synthase, CYP11B2 and 11-Hydroxylase, CYP11B1. *Int. J. Mol. Sci.* 24 (6), 5782. doi:10.3390/ijms24065782

Tang, M., Li, B., and Chen, H. (2023). Application of message passing neural networks for molecular property prediction. *Curr. Opin. Struct. Biol.* 81, 102616. doi:10.1016/j.sbi.2023.102616

Thiel, C., Schneckener, S., Krauss, M., Ghallab, A., Hofmann, U., Kanacher, T., et al. (2015). A systematic evaluation of the use of physiologically based pharmacokinetic modeling for cross-species extrapolation. *J. Pharm. Sci.* 104 (1), 191–206. doi:10.1002/jps.24214

Valentín-Goyco, J., Liu, J., Peng, H., Oommen, J., and Auchus, R. (2023). Selectivity of osilodrostat as an inhibitor of human steroidogenic cytochromes P450. *J. Steroid Biochem. Mol. Biol.* 231, 106316. doi:10.1016/j.jsbmb.2023.106316

Verma, S., Pandey, A., Pandey, A., Butler, J., Lee, J. S., Teoh, H., et al. (2024). Aldosterone and aldosterone synthase inhibitors in cardiorenal disease. *Am. J. Physiol. Heart Circ. Physiol.* 326 (3), H670–H688. doi:10.1152/ajpheart.00419.2023

Visan, A. I., and Negut, I. (2024). Integrating artificial intelligence for drug discovery in the context of revolutionizing drug delivery. *Life Basel, Switz.* 14 (2), 233. doi:10.3390/life14020233

Wang, Y., and Witten, I. H. (1997). "Inducing model trees for continuous classes," in *Proceedings of the ninth European conference on machine learning*, 128–137.

Weldon, S., Cerny, M., Gueneva-Boucheva, K., Cogan, D., Guo, X., Moss, N., et al. (2016). Selectivity of BI 689648, a novel, highly selective aldosterone synthase inhibitor: comparison with FAD286 and LCI699 in nonhuman primates. *J. Pharmacol. Exp. Ther.* 359 (1), 142–150. doi:10.1124/jpet.116.236463

Wendling, T., Dumitras, S., Ogungbenro, K., and Aarons, L. (2015). Application of a bayesian approach to physiological modelling of mavoglurant population pharmacokinetics. *J. Pharmacokinet. Pharmacodyn.* 42 (6), 639–657. doi:10.1007/s10928-015-9430-4

Wendling, T., Tsamandouras, N., Dumitras, S., Pigeolet, E., Ogungbenro, K., and Aarons, L. (2016). Reduction of a whole-body physiologically based pharmacokinetic model to stabilise the bayesian analysis of clinical data. *AAPS J.* 18 (1), 196–209. doi:10.1208/s12248-015-9840-7

Wu, K., Li, X., Zhou, Z., Zhao, Y., Su, M., Cheng, Z., et al. (2024). Predicting pharmacodynamic effects through early drug discovery with artificial intelligence-physiologically based pharmacokinetic (AI-PBPK) modelling. *Front. Pharmacol.* 15, 1330855. doi:10.3389/fphar.2024.1330855

Wu, Z., Pan, S., Chen, F., Long, G., Zhang, C., and Yu, P. S. (2021). A comprehensive survey on graph neural networks. *IEEE Trans. Neural Netw. Learn. Syst.* 32 (1), 4–24. doi:10.1109/TNNLS.2020.2978386

Zou, H., Banerjee, P., Leung, S., and Yan, X. (2020). Application of pharmacokinetic-pharmacodynamic modeling in drug delivery: development and challenges. *Front. Pharmacol.* 11, 997. doi:10.3389/fphar.2020.00997